ACS APPLIED MATERIALS & INTERFACES

Research Article

www.acsami.org

PEGylated Copper Nanowires as a Novel Photothermal Therapy Agent

Kuei-Chang Li, Hsun-Chen Chu, Yow Lin, Hsing-Yu Tuan,* and Yu-Chen Hu*

Department of Chemical Engineering, National Tsing Hua University, Hsinchu, Taiwan 300

Supporting Information

ABSTRACT: Metal nanowires are promising for their applications including electrical connectors, transparent conductive electrodes and conductive additives, but the use of metal nanowires as photothermal agents to convert light to heat has yet to be reported. Here we synthesized dispersible polyethylene glycol-coated (PEGylated) copper nanowires (CuNWs) and showed for the first time that PEGylated CuNWs were able to convert near-infrared (NIR, 808 nm) light into heat at a photothermal efficiency of 12.5%. The PEGylated CuNWs exhibited good reusability and enabled rapid temperature rise to >50 °C in 6 min by NIR irradiation. The PEGylated CuNWs were flexible and intertwined around the cancer cells, which, upon NIR irradiation, allowed for direct heat transmission to cells and effectively triggered cancer cell ablation *in vitro*. Intratumoral injection of PEGylated CuNWs into colon tumor-bearing mice and ensuing NIR irradiation for 6 min significantly raised the local temperature to >50 °C, induced necrosis, and suppressed tumor growth. Compared with other NIR light absorbing noble metal-based nanomaterials, PEGylated CuNWs are relatively easy to synthesize in both laboratory and large scales using the low cost copper. This study demonstrated the potential of PEGylated CuNWs as a new cost-effective photothermal agent, and paved a new avenue to using CuNWs for cancer therapy.

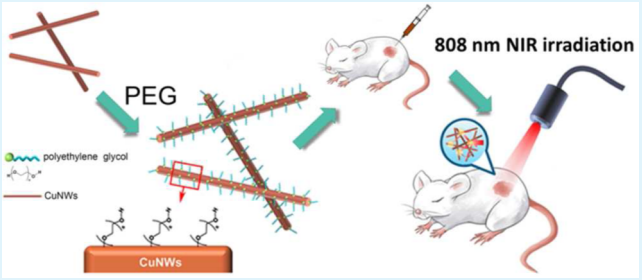

KEYWORDS: *copper nanowire, photothermal therapy, near-infrared, cancer therapy, PEGylated CuNWs, nanomaterial*

1. INTRODUCTION

Cancer is a leading cause of death worldwide. In recent years, laser-induced photothermal therapy (PTT) has captured increasing attention as a potent modality for cancer treatment,[1,2] which commonly utilizes the photothermal agent to convert near-infrared (NIR) light energy into heat to kill cancer cells. NIR light in the range of 700−900 nm (e.g., 808 nm) is minimally absorbed by skin and tissue, and allows deep (up to 10 cm) tissue penetration.[3−7] Consequently, the therapeutic effect occurs at the tumor site where both photothermal agent and localized photoirradiation coexist, thus conferring precise spatial-temporal selectivity.[8]

To date, organic and inorganic photothermal agents have been developed. Most organic photothermal agents are only activated by UV/visible light and are prone to photobleaching, thus limiting their applications.[9] Although carbon nanotubes and graphene oxide can be activated by NIR light and show high biocompatibility,[10,11] their photothermal conversion efficiency is low.[12] Inorganic photothermal agents such as gold (Au)-based nanostructures,[8,9,13] silver (Ag)-based nanomaterials,[14,15] platinum nanoparticles,[16] tungsten oxide nanorods,[17] and semimetal materials[18] have been developed. Among these inorganic photosensitizers, Au-based nanomaterials are the most extensively investigated due to their excellent biocompatibility and tunable surface plasmon resonance (SPR) property to convert NIR light into local heat.[8] However, the NIR absorbance of Au-based nanostructures diminishes after NIR laser irradiation, leading to low photostability[8] Recently, copper chalcogenide nanoparticles,[19] graphene oxide/copper sulfide nanocomposites,[12] copper sulfide nanocrystals,[20] ultrasmall PEGylated Cu_2-xS nanodots[21] and copper bismuth sulfide nanostructures[22] have also been developed.

Metal (e.g., Au, Ag, and Cu) nanowires are promising for their applications in electrical connectors, transparent conductive electrodes, and conductive additives thanks to their good electrical conductivity.[23] However, their uses on converting energy to heat have rarely been addressed despite their excellent thermal conductivity. Heat generation from metal nanowires may be driven by light or electricity. Although Ag nanowires have recently been exploited to convert electricity to heat via joule heating,[24] the use of metal nanowires as photothermal agents to convert light to heat has yet to be reported.

Herein, we report on the preparation of polyethylene glycol-coated (PEGylated) Cu nanowires (CuNWs) with efficient photothermal conversion (12.5%) by NIR irradiation at 808 nm, which enabled selective killing of cancer cells *in vitro* and effective photothermal ablation of cancers *in vivo* (Figure 1). In

Received: April 17, 2016
Accepted: April 25, 2016
Published: April 25, 2016

DOI: 10.1021/acsami.6b04579
ACS Appl. Mater. Interfaces 2016, 8, 12082−12090

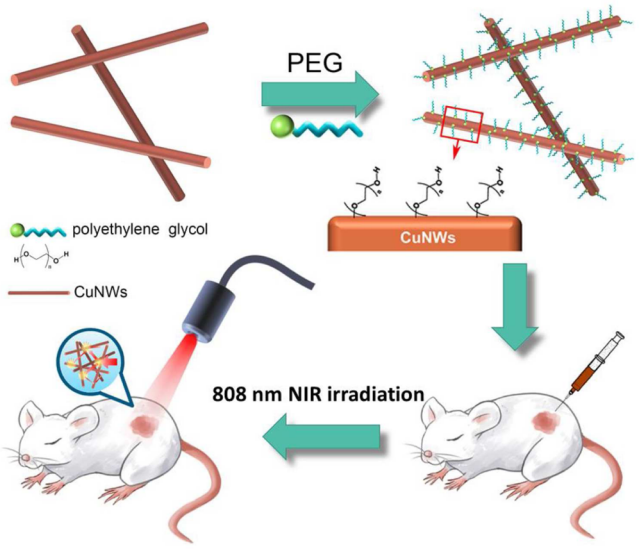

Figure 1. Scheme of PEGylated CuNWs as a photothermal agent for cancer therapy.

comparison with other NIR light absorbing noble metal-based nanomaterials (e.g., gold nanovesicles,[25] nanoparticles,[26] nanorods,[13,27] nanocages,[28] and nanoshells[29]), PEGylated CuNWs are relatively easy to synthesize in both laboratory and large scales and are composed of low cost copper element, rendering PEGylated CuNWs a promising candidate for cost-effective photothermal therapy.

2. MATERIALS AND METHODS

2.1. Chemicals and Cells. Oleylamine (OLA, 70%), ethanol (99.8%), toluene (99.9%), polyethylene glycol (PEG, average MW = 20 000), and tetrahydrofuran (THF, 99.9%) were purchased from Sigma-Aldrich. Copper chloride (CuCl, 99.99%) was purchased from Alfa. Hexane (ACS) was purchased from Macron Fine Chemicals. Mouse CT26 colon cancer cells were cultured in RPMI-1640 medium (Gibco) containing 10% fetal bovine serum (FBS, Hyclone) and 1% penicillin/streptomycin (Gibco). Mouse TRAMP-C1 prostate cancer cells were cultured in DMEM medium (Gibco) containing 10% FBS, 5 μg/mL bovine insulin (Sigma), 1×10^{-8} M dihydrotestosterone (Sigma), and 1% penicillin/streptomycin.

2.2. Synthesis of Copper Nanowires (CuNWs) and PEGylated CuNWs. CuNWs were synthesized in an organic solvent. Briefly, 300 mg of CuCl was added to a 50 mL three-neck flask inside the glovebox and sealed with rubber stoppers. The flask was removed from the glovebox and injected with 30 mL of oleylamine (70%). After the flask was connected to the Schlenk line and the mixture was purged with argon, the solution was heated to 110 °C for 50 min and magnetically stirred under inert atmosphere. The solution was subsequently heated and maintained at 250 °C for 50 min and the color changed to reddish brown. After it had cooled to room temperature, the reaction mixture was dispersed in hexane and centrifuged (8000 rpm, 5 min) 7 times to yield purified CuNWs.

For PEGylation, the aforementioned CuNWs (15 mg) were dispersed in 15 mL of THF, and 200 mg of PEG was added with stirring. The solution was heated and maintained at 50 °C for 4 h. When PEGylation was finished, the PEGylated CuNWs were purified by centrifugation and the precipitate was washed with ethanol 3 times. After drying, the PEGylated CuNWs were stored in powder form in the glovebox.

2.3. Measurement of Photothermal Performance. The PEGylated CuNWs were dispersed in water to a final concentration of 50 μg/mL and transferred to a quartz cuvette cell (1 cm in length, cat no: 143859, New Lab Start-Up). NIR laser beam (808 nm, power density 6 W/cm^2, total power 1.5 W) was conveyed through the cuvette, and the solution temperature was gauged with a thermocouple inserted into the solution. The calculation of photothermal performance is described in details in Supporting Information Methods.

2.4. CuNWs Characterization. The SEM images were taken with a field emission scanning electron microscope (SU8010, Hitachi). The low-resolution TEM images were obtained using a transmission electron microscope (H-7100, Hitachi). The high-resolution images were captured using a high-resolution transmission electron microscope (JEM-3000F, JEOL). SEM and TEM samples were prepared by dispersing the CuNWs in hexane or PEGylated CuNWs in ethanol at different concentrations. The solution was dropped onto the silicon wafer and carbon-coated copper grid for SEM and TEM characterization, respectively. X-ray diffraction (XRD) measurement of PEGylated CuNWs powder was carried out on a MAC Science MXP18 diffractometer with Cu Kα radiation. Absorbance of CuNWs (in toluene) and PEGylated CuNWs (in water) was measured with a UV−vis-NIR spectrophotometer (U-4100, Hitachi). Fourier transform infrared (FT-IR) spectra of CuNWs and PEGylated CuNWs were measured from samples in KBr pellets on an FT-IR spectrometer (Spectrum Two, PerkinElmer).

2.5. *In Vitro* Cytotoxicity and Photothermal Ablation by PEGylated CuNWs. For all *in vitro* and *in vivo* experiments, PEGylated CuNWs were dispersed in phosphate-buffered saline (PBS, pH 7.4). For cytotoxicity assay, cancer cells were seeded to 96-well plates (2×10^3 cells/well) and incubated with PEGylated CuNWs at different concentrations. After 1 h incubation, the PEGylated CuNWs supernatant was replaced with fresh medium and incubated for another 24 h, followed by MTT (3-[4,5-dimethylthiazol-2-yl]-2,5-diphenyltetrazolium bromide, Sigma) assays. For photothermal ablation, cancer cells were seeded to 12-well plates (2×10^5 cells/well) overnight and treated with 2.5 mg/mL of PEGylated CuNWs. After 1 h incubation, the supernatant was replaced with PBS (pH 7.4), followed by irradiation with NIR laser (808 nm, 1.5 W/cm^2) for 6 min. After irradiation, the cells were stained using the Live/Dead viability assay kit (Invitrogen). To quantify the percentage of cell death, the cells were stained with propidium iodide (PI, BD Biosciences), followed by flow cytometry (FACSCalibur, BD Biosciences) analysis.

2.6. SEM Analysis of Interactions between PEGylated CuNWs and Cells. CT26 cells were seeded onto Aclar embedding film coated with 0.1% gelatin, in 24-well plates (1×10^5 cells/well). After overnight culture, the cells were treated with 2.5 mg/mL of PEGylated CuNWs for 1 h and the supernatant was replaced with PBS, followed by irradiation with NIR laser (808 nm, 1.5 W/cm^2) for 6 min. Before and after NIR irradiation, the cells were prefixed in 2.5% glutaraldehyde for 1.5 h, washed twice with PBS, and fixed with 1% osmium tetraoxide for 1 h. The cells were dehydrated by ascending series of ethanol concentrations, and then were subjected to critical point drying (CPD) by Quorum K85. After CPD process, the cells were observed with an SEM (SU-8020, Hitachi).

2.7. *In Vivo* Photothermal Therapy by PEGylated CuNWs. Animal experiments were performed in compliance with the Guide for the Care and Use of Laboratory Animals (Ministry of Science and Technology, Taiwan), with the approval of the National Tsing Hua University Institutional Animal Care and Use Committee. Mouse CT26 cells were injected (5×10^5 cells/mouse) subcutaneously into the right abdomen of female BALB/c mice (6−8 weeks old, National Laboratory Animal Center, Taiwan). The width (W) and length (L) of the tumors were measured every 3 days, and the volume (V) was calculated by the formula: V (mm^3) = $L \times W^2 \times (\pi/6)$. When the tumor volume reached ≈50−60 mm^3 in 7 days (defined as day 0), the mice were anesthetized by intraperitoneal injection of Zoletil 50 (25 mg/kg body weight) and 2% Rompun (0.15 mL/kg body weight), followed by intratumoral injection of ≈50−60 μL of PBS or PEGylated CuNWs (2.5 mg/mL in PBS). At 1 h postinjection, the mice were irradiated with NIR laser (808 nm, 1.5 W/cm^2, n = 12 for each group) for 6 min. As a control, the mice received no NIR irradiation. The temperature changes within the tumors were recorded using the thermal imaging infrared camera (Avio). The mice were sacrificed at 15 days postirradiation.

DOI: 10.1021/acsami.6b04579
ACS Appl. Mater. Interfaces 2016, 8, 12082−12090

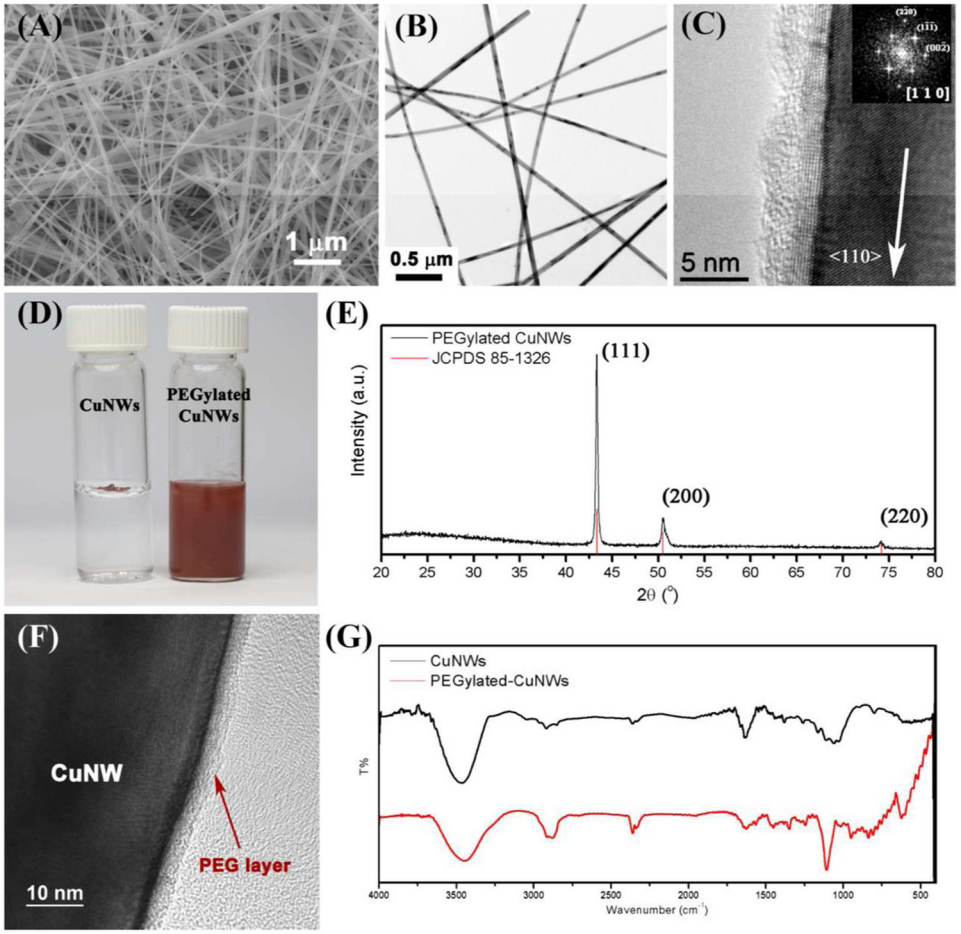

Figure 2. Characterization of CuNWs and PEGylated CuNWs. The SEM (A), TEM (B), high-resolution TEM (C) images, and FFT diffraction pattern (inset in panel C) of CuNWs are shown. The CuNWs and PEGylated CuNWs in water are shown in (D). (E) XRD pattern of PEGylated CuNWs. (F) High-resolution TEM image of PEGylated CuNWs. (G) FT-IR spectra of the CuNWs (black line) and PEGylated CuNWs (red line).

2.8. Immunohistochemical Staining. The tumor specimens were sectioned (thickness = 10 mm), fixed in methanol, washed, and blocked with the blocking buffer (0.1% Tween-20, 0.1 g/mL bovine serum albumin, 1% goat serum in PBS, pH 7.4) for 30 min, followed by incubation with the rabbit anti-mouse MAb specific for HMGB1 (1:50 dilution, Abcam) at 4 °C overnight. After 3 washes, the sections were incubated with goat anti-rabbit IgG (1:200 dilution, Jackson ImmunoResearch) conjugated with Alexa 488 for 1 h at room temperature. The nuclei were stained by DAPI (Vector Laboratories). The confocal microscopic images were captured and 5 random images (for each group) were processed using Image Pro Plus 6.0 (Media Cybernetics). Dividing the HMGB1-positive pixels by the DAPI pixels yielded the percentages of $HMGB1^+$ cells.

2.9. Statistical Analysis. All quantitative data were analyzed using one-way analysis of variance (ANOVA) or Student's *t*-test using a two-tailed distribution. The *in vitro* data represent the means ± SD of at least 3 independent experiments. $p < 0.05$ was considered significant.

3. RESULTS AND DISCUSSION

3.1. Synthesis and Characterization of CuNWs and PEGylated CuNWs. The CuNWs were synthesized via a heating-up method in organic solvent.[30,31] The precursor CuCl (300 mg) was dissolved in 30 mL of oleylamine. Cu^0 was generated via a disproportionation reaction at 250 °C and CuNWs were grown from a self-seeded growth with a five-fold twinned structure. The obtained CuNWs were straight, densely and uniformly distributed with smooth surface, as revealed by the SEM (Figure 2A) and low-resolution TEM (Figure 2B) images. On average, the CuNWs were ≈46 nm in diameter and ≈40 μm in length as measured from more than 100 wires. The high-resolution TEM (HR-TEM) image further revealed oleylamine-capped layer on the surface of wire and a well-developed crystalline structure (Figure 2C). The corresponding fast Fourier transform (FFT) diffraction pattern (inset of Figure 2C) of a nanowire viewed along [110] zone axis indicated that the nanowire grew along ⟨110⟩ growth direction.

However, oleylamine-capped CuNWs were not dispersible in water and tended to aggregate on the surface of water due to their hydrophobic characteristics (Figure 2D). To disperse CuNWs in aqueous solution, the as-prepared CuNWs were functionalized by polyethylene glycol (PEG), an FDA-approved polymer often used for functionalize or stabilize biomolecules.[32] CuNWs after PEGylation were homogeneously dispersed in water (Figure 2D), confirming that PEGylation turned CuNWs from hydrophobic to hydrophilic and enabled CuNWs to be dispersed in polar solvents such as water and ethanol. The zeta potential of PEGylated CuNWs was ≈−16.8 mV in water.

Figure 2E depicts the XRD patterns of PEGylated CuNWs and the standard Cu on JCPDS (no. 85-1326). Three obvious peaks appeared at 2θ = 43.3°, 50.6°, and 74.3°, which, respectively, represented the (111), (200), and (220) crystal planes in face-centered-cubic (fcc) of crystalline Cu metal. According to the XRD pattern, the crystal structure of CuNWs after PEGylation remained secure. HR-TEM image (Figure 2F)

DOI: 10.1021/acsami.6b04579
ACS Appl. Mater. Interfaces 2016, 8, 12082−12090

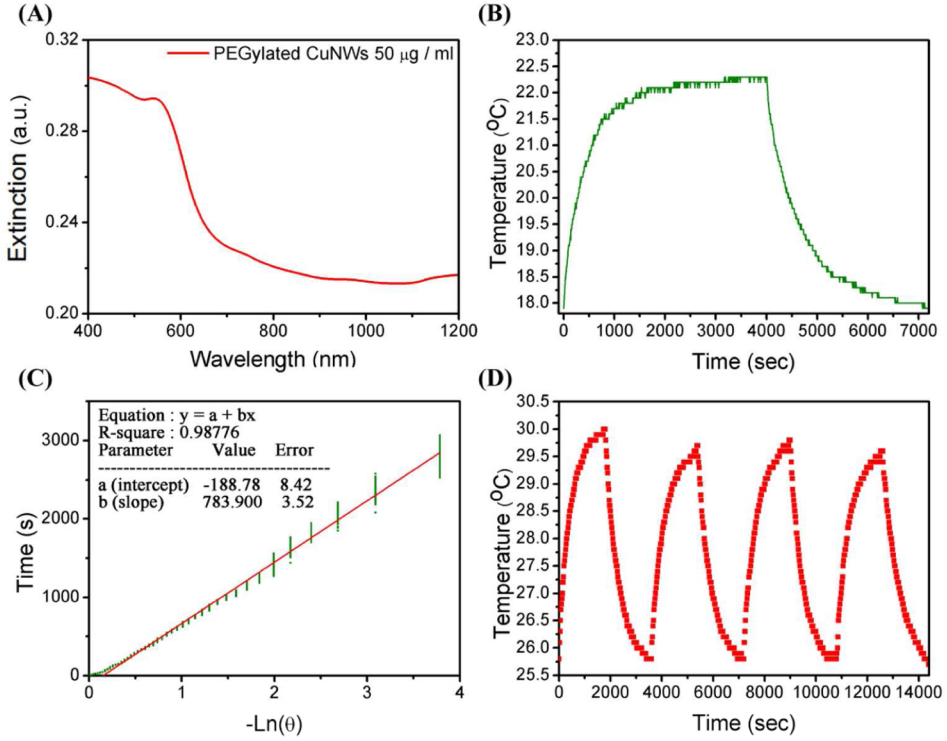

Figure 3. Photothermal conversion performance of PEGylated CuNWs. (A) Absorption spectrum of the PEGylated CuNWs dispersed in water (50 μg/mL) in the quartz cuvette cell. (B) Photothermal effect of the PEGylated CuNWs. Three milliliters of PEGylated CuNWs aqueous solution (50 μg/mL) in the quartz cuvette cell (1 cm in length) was irradiated by an 808 nm semiconductor laser diode (total power 1.5 W) for 4000 s and the laser was turned off. (C) Linear time data from the cooling period (after 4000 s in panel B) vs negative natural logarithm of driving force temperature. τ_S is the slope of the linear line, which is 783.9 s. (D) Temperature change of PEGylated CuNWs aqueous solution over 4 laser irradiation on/off cycles.

illustrated that a uniform PEG layer was capped on the surface of CuNWs, whereas the internal structure of CuNWs was unchanged. Figure 2G shows the Fourier transform infrared (FT-IR) spectra of CuNWs before (black line) and after (red line) PEGylation. Both spectra of CuNWs and PEGylated CuNWs displayed a strong and broad band at ≈3440 cm^{-1}, which mainly originated from the stretching vibration of O−H bond in PEG and the N−H stretching in oleylamine, respectively.[33] The bands at 1632 cm^{-1} assigned to bending modes of the hydroxyl groups of adsorbed water. The bands at 2917 and 2852 cm^{-1} of PEGylated CuNWs corresponded to asymmetric and symmetric stretching vibration of alkyl (CH_2) chain in PEG, respectively. The band at 1100 cm^{-1} was attributed to the C−O stretching vibration in PEG. Compared with the peak (1107 cm^{-1}) in IR spectrum of pure PEG,[34] there was a ≈7 cm^{-1} shift to lower wavenumber, suggesting that interactions between PEG and CuNWs were formed.[34]

3.2. Photothermal Conversion Performance of PEGylated CuNWs. Figure 3A shows the UV−vis-NIR spectrum of PEGylated CuNWs in water (50 μg/mL) in the wavelength range from 400 to 1200 nm, which revealed that the light absorption by PEGylated CuNWs gradually increased from 1100 to 585 nm. To measure the photothermal conversion performance at 808 nm, 3.5 mL of PEGylated CuNWs solution (50 μg/mL) in the quartz cuvette cell (1 cm in length) was irradiated by an 808 nm semiconductor laser diode with a total power of 1.5 W. As shown in Figure 3B, the temperature of PEGylated CuNWs solution rose 4.4 °C from 17.9 to 22.3 °C in 4000 s, confirming the capability of PEGylated CuNWs to convert NIR light energy to heat.

The energy balance equation of system can be described as follows:[35]

$$\sum_i m_i C_{pi} \frac{d\Delta T}{dt} = Q_{NW} + Q_{dis} - Q_{surr}$$

where m_iCp_i are products of mass and heat capacity of quartz cuvette cell, PEGylated CuNWs and water in the system, ΔT is the temperature difference between the system and surrounding, and t is time. Q_{NW} is the energy converted by PEGylated CuNWs from the radiant energy. Q_{dis} is the energy input by the cuvette cell which absorbs the energy from laser beam, and Q_{surr} represents the energy loss from system to surrounding through the outer surface of quartz cuvette. On the basis of the foregoing equation, the photothermal conversion efficiency η was calculated using the following equation:[35]

$$\eta = \frac{hA(T_{MAX} - T_{surr}) - Q_{dis}}{I(1 - 10^{-A_{808}})}$$

where T_{MAX} is temperature of the system at steady state, T_{surr} is temperature of the surrounding, I is the power of the laser beam (1.5 W), A_{808} is the absorbance at 808 nm (≈0.22), h and A are heat transfer and the surface area of the quartz curvet cell, respectively. When PEGylated CuNWs solution was replaced with equal volume of deionized water, Q_{dis} was measured to be 8.4 mW.

According to Figure 3C, the value of $+hA$ was calculated to be 18.7 mW/°C (see Supporting Information Methods for the details of calculation). On the basis of the above equation, the photothermal conversion of PEGylated CuNWs was deter-

DOI: 10.1021/acsami.6b04579
ACS Appl. Mater. Interfaces 2016, 8, 12082−12090

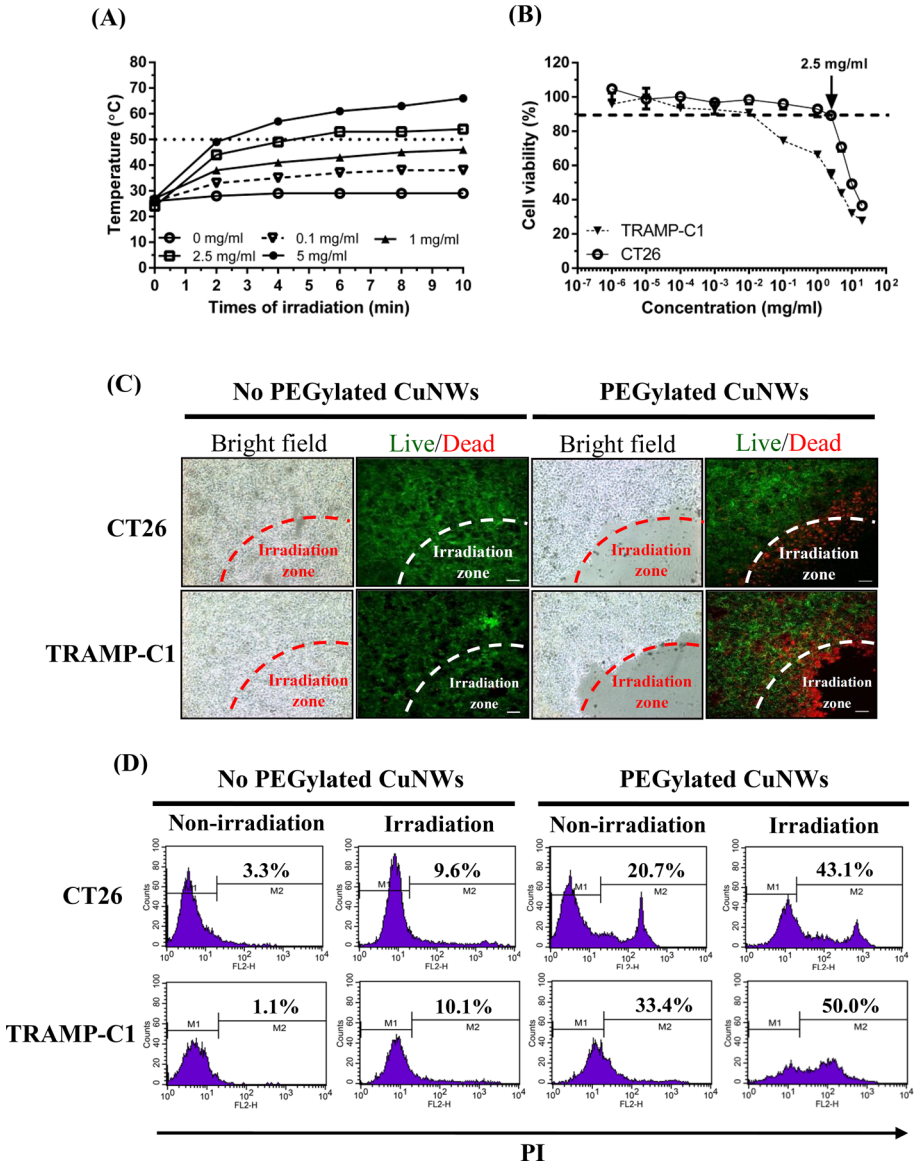

Figure 4. *In vitro* photothermal effect of PEGylated CuNWs. (A) Temperature elevation of PEGylated CuNWs (0−5 mg/mL, in 0.5 mL PBS) under NIR laser irradiation within 10 min (808 nm, 1.5 W/cm^2). (B) Cytotoxicity of PEGylated CuNWs on CT26 and TRAMP-C1 cell as measured by MTT assay. (C) Cell death analysis by Live/Dead staining. (D) Cell death analysis by PI staining/flow cytometry. In all experiments, PEGylated CuNWs were dispersed in PBS. For *in vitro* tumor cell ablation, we incubated CT26 and TRAMP-C1 cells in 12-well plates (2 × 10^5 cells/well) with or without 2.5 mg/mL of PEGylated CuNWs (1 mL/well) for 1 h, and exposed the cells to local NIR laser irradiation (808 nm, 1.5 W/cm^2) for 6 min. After irradiation, the cells were subjected to Live/Dead staining (C) or PI staining/flow cytometry (D). The red and green fluorescence indicated dead and viable cells, respectively.

mined to be 12.5% under irradiation by an 808 nm laser. This light-to-heat conversion efficiency was high enough for the photothermal therapy of cancer cells. To test the reusability, the PEGylated CuNWs were subjected to 4 cycles of temperature rising and lowering. In each cycle, the difference between adjacent peak temperature was within ±0.5 °C (Figure 3D), which attested that PEGylated CuNWs withstand repeated and long-time irradiation and exhibited good reusability.

3.3. *In Vitro* Photothermal Effects of PEGylated CuNWs. It is known that tumor cells can be ablated upon exposure at 42 °C for 15−60 min, yet the duration time can be shortened to 4−6 min when the temperature is >50 °C;[36] thus, the ability to raise the temperature to >50 °C is desired. To evaluate whether PEGylated CuNWs conferred photothermal effects potent enough to elevate the temperature >50 °C, we irradiated different concentrations of PEGylated CuNWs (0−5 mg/mL, in 0.5 mL PBS) in microfuge tubes with NIR laser (808 nm). As shown in Figure 4A, the temperature increased with irradiation time and the magnitude was positively correlated with the PEGylated CuNWs concentrations. When the PEGylated CuNWs concentrations were <2.5 mg/mL, the temperature failed to reach 50 °C after 10 min exposure. With 2.5 and 5 mg/mL of CuNWs, in 6 min the temperature exceeded 50 and 60 °C, respectively.

To assess the cytotoxicity of PEGylated CuNWs on cancer cells, we incubated colon (CT26) and prostate (TRAMP-C1) cancer cells in 96-well plates (2 × 10^3 cells/well) with different concentrations of PEGylated CuNWs. The MTT assay (Figure 4B) revealed that CT26 and TRAMP-C1 cells were tolerant to PEGylated CuNWs at concentrations ≤0.01 mg/mL but the

DOI: 10.1021/acsami.6b04579
ACS Appl. Mater. Interfaces 2016, 8, 12082−12090

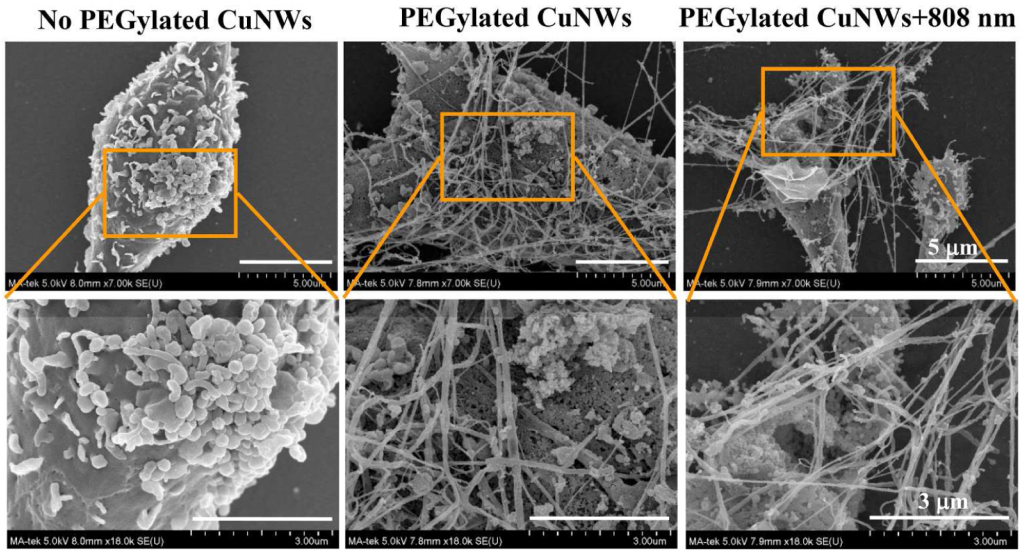

Figure 5. SEM image of CT26 cells interaction with PEGylated CuNWs. The cells were incubated with 2.5 mg/mL of PEGylated CuNWs for 1 h, with or without subsequent NIR laser irradiation for 6 min. As a control, the cells were not incubated with PEGylated CuNWs.

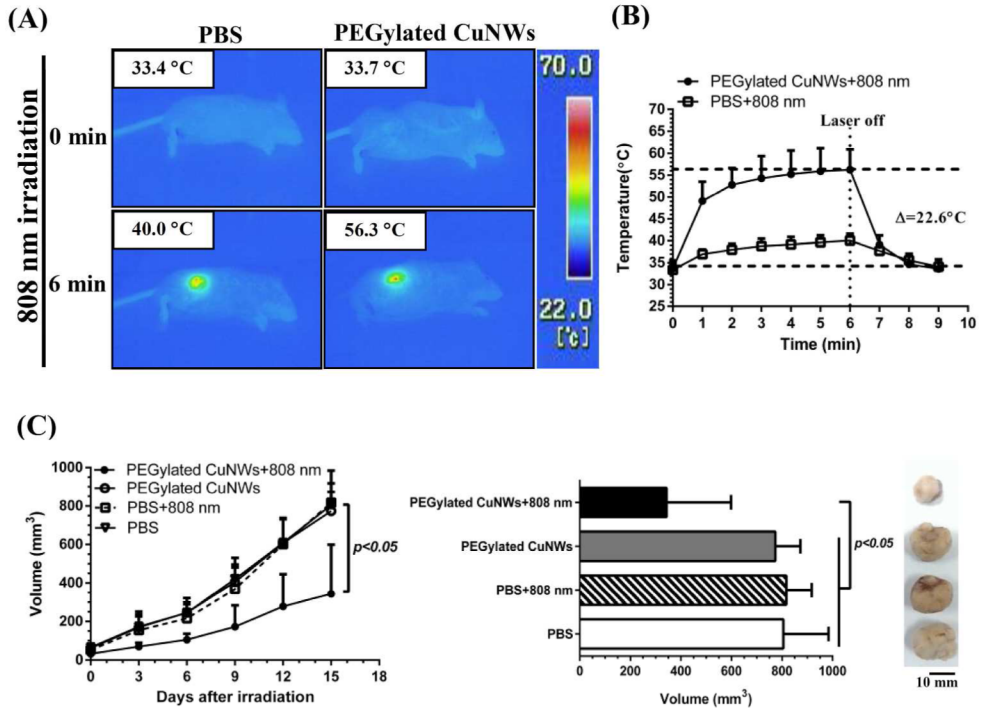

Figure 6. *In vivo* photothermal therapy efficacy of PEGylated CuNWs. (A) Thermal imaging of tumor-bearing BALB/c mice. (B) Temperature profiles of tumor-bearing BALB/c mice. (C) Tumor volume of CT26-bearing BALB/c mice after PEGylated CuNWs-mediated photothermal ablation. The colon cancer cells (CT26) were injected subcutaneously into BALB/c mice. When the tumor volume reached 50−60 mm^3, the mice were divided into 4 groups (n = 12 for each group) and were intratumorally injected with ≈50−60 μL of PBS or PEGylated CuNWs (2.5 mg/mL in PBS), with or without NIR laser irradiation (808 nm, 1.5 W/cm^2, 6 min). At 6 min postirradiation, the laser was turned off and the temperature was monitored for another 3 min. The temperature changes within the tumors were recorded using the thermal imaging infrared camera and the average temperatures are shown. The tumor volume was recorded throughout the experiment and the data represent mean ± SD. At 15 days postirradiation, the mice were sacrificed and tumor specimens were removed.

TRAMP-C1 viability decreased precipitously at >0.01 mg/mL of PEGylated CuNWs. In contrast, the CT26 viability did not drop sharply until the PEGylated CuNWs concentration was elevated to >2.5 mg/mL (Figure 4B). Since 2.5 mg/mL of PEGylated CuNWs enabled rapid temperature rise to >50 °C without excessive cytotoxicity to CT26 and primary cells such as adipose-derived stem cells (Figure S1), we chose 2.5 mg/mL for subsequent experiments.

To evaluate the capability of PEGylated CuNWs for *in vitro* tumor cell ablation, we incubated CT26 and TRAMP-C1 cells in 12-well plates (2 × 10^5 cells/well) with or without 2.5 mg/mL of PEGylated CuNWs (1 mL/well) for 1 h, and exposed the cells to local NIR laser irradiation (808 nm, 1.5 W/cm^2) for

DOI: 10.1021/acsami.6b04579
ACS Appl. Mater. Interfaces 2016, 8, 12082−12090

6 min. The ensuing bright field microscopy and Live/Dead staining assay (Figure 4C) illustrated negligible death of CT26 and TRAMP-C1 cells without PEGylated CuNWs. In contrast, PEGylated CuNWs and NIR irradiation evoked local cell ablation and significant cell death (indicated by red fluorescence) within and near the irradiation zone, but without apparent damage to cells outside the irradiation zone. The PI staining and flow cytometry (Figure 4D) further revealed low percentages of death for the cells incubated in the absence of PEGylated CuNWs, with or without irradiation. Strikingly, PEGylated CuNWs and NIR irradiation led to 43.1% and 50.0% of dead CT26 and TRAMP-C1 cells, respectively. These death rates were significantly ($p < 0.05$) higher than those of nonirradiated cells that were incubated with PEGylated CuNWs, hence demonstrating the potential of PEGylated CuNWs as a photothermal agent to induce cancer cell death under NIR laser irradiation.

3.4. Interaction between PEGylated CuNWs and Cells. To examine whether PEGylated CuNWs directly interacted with the cancer cells, we incubated the CT26 cells with PEGylated CuNWs for 1 h with or without exposure to NIR laser irradiation for 6 min. After cell fixation, the CT26 cells were subjected to SEM analysis (Figure 5). As shown, abundant PEGylated CuNWs were observed to intertwine around the cells, indicating that the PEGylated CuNWs were flexible enough to intimately contact with the cell surface. After NIR irradiation, membrane disintegration and cell destruction were evident, which agreed with the cell death triggered by CuNWs and NIR irradiation (Figure 4C,D). The close contact between PEGylated CuNWs and cells allowed for direct heat transmission to cells, hence effectively causing the protein denaturation, DNA damage and eventual cell death.

Intriguingly, cancer cells such as HeLa can internalize gold nanowires and the uptake efficiency depends on the nanowire length.[37] Conversely, microglial cell (an immune cell in the brain) is capable of breaking apart and internalizing micron-sized extracellular agglomerates of multiwalled carbon nanotube.[38] Here the length of CuNWs was ≈40 μm. Whether the PEGylated CuNWs can be broken apart and engulfed by CT26 or TRAMP-C1 cells awaits further investigation.

3.5. *In Vivo* Photothermal Therapy Efficacy of PEGylated CuNWs. To evaluate the potential of PEGylated CuNWs for *in vivo* photothermal therapy, we injected CT26 cells subcutaneously into BALB/c mice and divided the mice into 4 groups ($n = 12$ for each group) when the tumor volume reached 50–60 mm^3. The mice were intratumorally injected with ≈50–60 μL of PBS or PEGylated CuNWs (2.5 mg/mL), with or without NIR laser irradiation (808 nm, 1.5 W/cm^2, 6 min). The injection of PEGylated CuNWs did not significantly affect the mice body weight regardless of NIR irradiation (Figure S2), suggesting low side effects.

With NIR irradiation, the local temperature at the tumor (Figure 6A,B) in the mice receiving no PEGylated CuNWs only increased from 33.4 °C (0 min) to 40.0 °C (6 min). In contrast, CuNWs plus NIR irradiation provoked fast temperature rise, which increased sharply from 33.7 to 56.3 °C ($\Delta T \approx$ 22.6 °C) in 6 min. After the laser was switched off, the temperature rapidly dropped below 40.0 °C within 3 min (Figure 6B). Importantly, PEGylated CuNWs in conjunction with NIR irradiation significantly suppressed the tumor progression while PEGylated CuNWs alone and PBS alone failed to repress the tumor growth (Figure 6C). Compared with the tumor volume in other groups, the tumor volume in the mice that received PEGylated CuNWs and NIR irradiation was significantly lower (343.8 ± 254.6 mm^3 at 15 days postirradiation, Figure 6C). Figure 6 collectively confirms that PEGylated CuNWs converted NIR light energy into heat and conferred photothermal therapeutic effects.

Heat treatment can lead to tumor cell death via cellular structure disruption, apoptosis, and/or necrosis[20,39] and it is more likely to induce necrosis than apoptosis above a threshold temperature (46 °C).[1] To examine whether the PEGylated CuNWs-mediated thermal therapy induced necrosis, the tumor specimens were removed at 15 days postirradiation, sectioned, and immunostained for the release of the necrosis marker HMGB1 (high-mobility group box 1 protein). The immunofluorescence microscopy (Figure 7A) and quantitative analysis

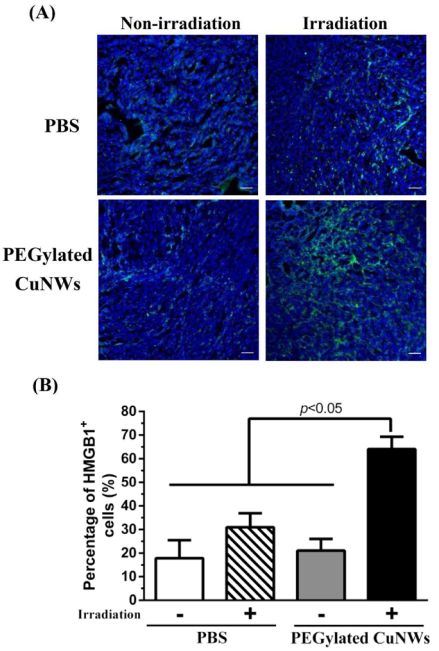

Figure 7. PEGylated CuNWs-mediated photothermal therapy induced necrosis. (A) Tumor necrosis analysis by HMGB1-specific immunostaining. (B) Percentage of HMGB1$^+$ cells in the tumor tissue. The tumor specimens removed at 15 days postirradiation as in Figure 6 were sectioned and immunostained for HMGB1. The number of HMGB1$^+$ cells were quantified from 5 fields from each group and divided by the total number of cells (DAPI$^+$ cells) to yield the percentage of HMGB1$^+$ cells. Scale bar = 50 μm.

(Figure 7B) revealed that PEGylated CuNWs in combination with NIR irradiation induced evident HMGB1 release in up to 64.1% of cells, whereas the percentages of HMGB1-releasing cells were <30% in other groups, confirming that necrosis contributed to the tumor cell death during the photothermal therapy.

Such induction of necrosis and HMGB1 release is crucial to cancer therapy because necrotic cells release various damage-associated molecular pattern (DAMP) molecules such as HMGB1, calreticulin (CRT) and ATP.[12,40] In particular, HMGB1 can interact with pattern recognition receptors,[41] promote cytokine production,[42] recruit immune cells[43] and modulate dendritic cells maturation.[44] These characteristics render HMGB1 a powerful adjuvant to potentiate antitumor immunity and activate effector T cells to kill the residual tumor cells, in addition to direct thermal ablation.

DOI: 10.1021/acsami.6b04579
ACS Appl. Mater. Interfaces 2016, 8, 12082–12090

Taken together, CuNWs are stable, highly electrically conductive and have been exploited as sensors, nanoprobes, optical devices, transparent conducting electrodes and deformable conductors thanks to their high conductivity, mechanical flexibility, and cost effectiveness (for review see refs 23 and 30). Here we demonstrated for the first time the application of PEGylated CuNWs as a photothermal agent. Copper is the third most abundant element on earth and can be obtained at low cost. Compared with other NIR light absorbing noble metal-based nanomaterials, PEGylated CuNWs are cheap and easy to synthesize in both laboratory and larger scales. These features render PEGylated CuNWs a novel and promising nanomaterial for photothermal therapy. The therapeutic efficacy can be further improved by conjugating additional anticancer drugs such as doxorubicin.[8] The PEG layer on the PEGylated CuNWs surface not only enabled PEGylated CuNWs dispersion, but also allowed for facile conjugation of anticancer drugs. The high aspect ratio of PEGylated CuNWs provides large surface area for loading of multiple drug molecules, thereby making it feasible to combine PEGylated CuNWs-based photothermal therapy and chemotherapy for cancer treatment. One possible drawback of CuNWs is the large size because large-sized nanomaterials are difficult to be cleared from the body[16] and cannot be systemically administered and accumulate in the tumors via enhanced permeability and retention (EPR) effect.[18] Relevant experiments assessing the systemic biodistribution, biocompatibility, and clearance of PEGylated CuNWs are ongoing. Whether shorter PEGylated CuNWs can be more readily cleared and how the PEGylated CuNWs length influences the photothermal conversion and thermal ablation efficacy will be explored.

4. CONCLUSIONS

We demonstrated for the first time that PEGylated CuNWs can effectively convert NIR light to heat at an efficiency of 12.5%. The PEGylated CuNWs exhibited good reusability and enabled rapid temperature rise to >50 °C in 6 min by NIR (808 nm) irradiation. The PEGylated CuNWs were flexible and were able to intertwine around the cancer cells, which, upon NIR irradiation, allowed for direct heat transmission to cells and effectively triggered cancer cell ablation *in vitro*. Intratumoral injection of PEGylated CuNWs into colon tumor-bearing mice and ensuing NIR irradiation (808 nm, 1.5 W/cm^2) for 6 min significantly raised the local temperature to >50 °C, induced necrosis and suppressed tumor growth. The PEGylated CuNWs can be synthesized by a simple approach using the low cost copper, rendering PEGylated CuNWs an attractive photothermal agent. This study demonstrates the potential of PEGylated CuNWs as an agent for cancer photothermal therapy and paves a new avenue to the applications of metal nanowires.

■ ASSOCIATED CONTENT

Supporting Information

The Supporting Information is available free of charge on the ACS Publications website at DOI: 10.1021/acsami.6b04579.

The photothermal conversion efficiency of PEGylated CuNWs calculated by energy balance equation; the cytotoxicity of PEGylated CuNWs in Adipose-derived stem cells (rASCs) and CT26 cells evaluated by MTT assays; the mouse body weight after PEGylated CuNWs injection and NIR laser irradiation, recorded every 3 days (PDF)

■ AUTHOR INFORMATION

Corresponding Authors

*Phone: (886)3-572-3661. Fax: (886)3-571-5408. E-mail: hytuan@che.nthu.edu.tw.

*Phone: (886)3-571-8245. Fax: (886)3-571-5408. E-mail: ychu@mx.nthu.edu.tw.

Notes

The authors declare no competing financial interest.

■ ACKNOWLEDGMENTS

This work was supported by the National Tsing Hua University (Toward World-Class University Project 104N2050E1 and 105N526CE1) and Ministry of Science and Technology (MOST 103-2221-E-007-093-MY3), Taiwan.

■ REFERENCES

(1) Frazier, N.; Ghandehari, H. Hyperthermia Approaches for Enhanced Delivery of Nanomedicines to Solid Tumors. *Biotechnol. Bioeng.* **2015**, *112* (10), 1967−1983.

(2) Biju, V. Chemical Modifications and Bioconjugate Reactions of Nanomaterials for Sensing, Imaging, Drug Delivery and Therapy. *Chem. Soc. Rev.* **2014**, *43* (3), 744−764.

(3) Melancon, M. P.; Zhou, M.; Li, C. Cancer Theranostics with near-Infrared Light-Activatable Multimodal Nanoparticles. *Acc. Chem. Res.* **2011**, *44* (10), 947−956.

(4) Yang, K.; Zhang, S.; Zhang, G.; Sun, X.; Lee, S. T.; Liu, Z. Graphene in Mice: Ultrahigh in Vivo Tumor Uptake and Efficient Photothermal Therapy. *Nano Lett.* **2010**, *10* (9), 3318−3323.

(5) Weissleder, R. A Clearer Vision for in Vivo Imaging. *Nat. Biotechnol.* **2001**, *19* (4), 316−317.

(6) Kobayashi, H.; Longmire, M. R.; Ogawa, M.; Choyke, P. L. Rational Chemical Design of the Next Generation of Molecular Imaging Probes Based on Physics and Biology: Mixing Modalities, Colors and Signals. *Chem. Soc. Rev.* **2011**, *40* (9), 4626−4648.

(7) Zhang, Z.; Wang, J.; Chen, C. Near-Infrared Light-Mediated Nanoplatforms for Cancer Thermo-Chemotherapy and Optical Imaging. *Adv. Mater.* **2013**, *25* (28), 3869−3880.

(8) Wang, D. G.; Xu, Z. A.; Yu, H. J.; Chen, X. Z.; Feng, B.; Cui, Z. R.; Lin, B.; Yin, Q.; Zhang, Z. W.; Chen, C. Y.; Wang, J.; Zhang, W.; Li, Y. P. Treatment of Metastatic Breast Cancer by Combination of Chemotherapy and Photothermal Ablation Using Doxorubicin-Loaded DNA Wrapped Gold Nanorods. *Biomaterials* **2014**, *35* (29), 8374−8384.

(9) Vijayaraghavan, P.; Liu, C. H.; Vankayala, R.; Chiang, C. S.; Hwang, K. C. Designing Multi-Branched Gold Nanoechinus for Nir Light Activated Dual Modal Photodynamic and Photothermal Therapy in the Second Biological Window. *Adv. Mater.* **2014**, *26* (39), 6689−6695.

(10) Tao, Y.; Ju, E.; Ren, J.; Qu, X. Immunostimulatory Oligonucleotides-Loaded Cationic Graphene Oxide with Photothermally Enhanced Immunogenicity for Photothermal/Immune Cancer Therapy. *Biomaterials* **2014**, *35* (37), 9963−9971.

(11) Wang, C.; Xu, L.; Liang, C.; Xiang, J.; Peng, R.; Liu, Z. Immunological Responses Triggered by Photothermal Therapy with Carbon Nanotubes in Combination with Anti-Ctla-4 Therapy to Inhibit Cancer Metastasis. *Adv. Mater.* **2014**, *26* (48), 8154−8162.

(12) Bai, J.; Liu, Y.; Jiang, X. Multifunctional Peg-Go/Cus Nanocomposites for near-Infrared Chemo-Photothermal Therapy. *Biomaterials* **2014**, *35* (22), 5805−5813.

(13) Li, X.; Takashima, M.; Yuba, E.; Harada, A.; Kono, K. Pegylated Pamam Dendrimer-Doxorubicin Conjugate-Hybridized Gold Nanorod for Combined Photothermal-Chemotherapy. *Biomaterials* **2014**, *35* (24), 6576−6584.

DOI: 10.1021/acsami.6b04579
ACS Appl. Mater. Interfaces 2016, 8, 12082−12090

(14) Noh, M. S.; Lee, S.; Kang, H.; Yang, J. K.; Lee, H.; Hwang, D.; Lee, J. W.; Jeong, S.; Jang, Y.; Jun, B. H.; Jeong, D. H.; Kim, S. K.; Lee, Y. S.; Cho, M. H. Target-Specific near-Ir Induced Drug Release and Photothermal Therapy with Accumulated Au/Ag Hollow Nanoshells on Pulmonary Cancer Cell Membranes. *Biomaterials* **2015**, *45*, 81−92.
(15) Shi, J.; Wang, L.; Zhang, J.; Ma, R.; Gao, J.; Liu, Y.; Zhang, C.; Zhang, Z. A Tumor-Targeting near-Infrared Laser-Triggered Drug Delivery System Based on Go@Ag Nanoparticles for Chemo-Photothermal Therapy and X-Ray Imaging. *Biomaterials* **2014**, *35* (22), 5847−5861.
(16) Wang, C.; Cai, X.; Zhang, J.; Wang, X.; Wang, Y.; Ge, H.; Yan, W.; Huang, Q.; Xiao, J.; Zhang, Q.; Cheng, Y. Trifolium-Like Platinum Nanoparticle-Mediated Photothermal Therapy Inhibits Tumor Growth and Osteolysis in a Bone Metastasis Model. *Small* **2015**, *11* (17), 2080−2086.
(17) Zhou, Z.; Kong, B.; Yu, C.; Shi, X.; Wang, M.; Liu, W.; Sun, Y.; Zhang, Y.; Yang, H.; Yang, S. Tungsten Oxide Nanorods: An Efficient Nanoplatform for Tumor Ct Imaging and Photothermal Therapy. *Sci. Rep.* **2014**, *4*, 3653.
(18) Li, W.; Rong, P.; Yang, K.; Huang, P.; Sun, K.; Chen, X. Semimetal Nanomaterials of Antimony as Highly Efficient Agent for Photoacoustic Imaging and Photothermal Therapy. *Biomaterials* **2015**, *45*, 18−26.
(19) Zhou, M.; Zhang, R.; Huang, M.; Lu, W.; Song, S.; Melancon, M. P.; Tian, M.; Liang, D.; Li, C. A Chelator-Free Multifunctional [64cu]Cus Nanoparticle Platform for Simultaneous Micro-Pet/Ct Imaging and Photothermal Ablation Therapy. *J. Am. Chem. Soc.* **2010**, *132* (43), 15351−15358.
(20) Wang, S.; Riedinger, A.; Li, H.; Fu, C.; Liu, H.; Li, L.; Liu, T.; Tan, L.; Barthel, M. J.; Pugliese, G.; De Donato, F.; Scotto D'Abbusco, M.; Meng, X.; Manna, L.; Meng, H.; Pellegrino, T. Plasmonic Copper Sulfide Nanocrystals Exhibiting near-Infrared Photothermal and Photodynamic Therapeutic Effects. *ACS Nano* **2015**, *9* (2), 1788−1800.
(21) Mou, J.; Li, P.; Liu, C.; Xu, H.; Song, L.; Wang, J.; Zhang, K.; Chen, Y.; Shi, J.; Chen, H. Ultrasmall Cu2-Xs Nanodots for Highly Efficient Photoacoustic Imaging-Guided Photothermal Therapy. *Small* **2015**, *11* (19), 2275−2283.
(22) Li, B.; Ye, K.; Zhang, Y.; Qin, J.; Zou, R.; Xu, K.; Huang, X.; Xiao, Z.; Zhang, W.; Lu, X.; Hu, J. Photothermal Theragnosis Synergistic Therapy Based on Bimetal Sulphide Nanocrystals Rather Than Nanocomposites. *Adv. Mater.* **2015**, *27* (8), 1339−1345.
(23) Ravi Kumar, D. V.; Woo, K.; Moon, J. Promising Wet Chemical Strategies to Synthesize Cu Nanowires for Emerging Electronic Applications. *Nanoscale* **2015**, *7* (41), 17195−17210.
(24) Kim, T.; Kim, Y. W.; Lee, H. S.; Kim, H.; Yang, W. S.; Suh, K. S. Uniformly Interconnected Silver-Nanowire Networks for Transparent Film Heaters. *Adv. Funct. Mater.* **2013**, *23* (10), 1250−1255.
(25) Huang, P.; Lin, J.; Li, W.; Rong, P.; Wang, Z.; Wang, S.; Wang, X.; Sun, X.; Aronova, M.; Niu, G.; Leapman, R. D.; Nie, Z.; Chen, X. Biodegradable Gold Nanovesicles with an Ultrastrong Plasmonic Coupling Effect for Photoacoustic Imaging and Photothermal Therapy. *Angew. Chem., Int. Ed.* **2013**, *52* (52), 13958−13964.
(26) Jing, L.; Liang, X.; Deng, Z.; Feng, S.; Li, X.; Huang, M.; Li, C.; Dai, Z. Prussian Blue Coated Gold Nanoparticles for Simultaneous Photoacoustic/Ct Bimodal Imaging and Photothermal Ablation of Cancer. *Biomaterials* **2014**, *35* (22), 5814−5821.
(27) Yang, H. W.; Liu, H. L.; Li, M. L.; Hsi, I. W.; Fan, C. T.; Huang, C. Y.; Lu, Y. J.; Hua, M. Y.; Chou, H. Y.; Liaw, J. W.; Ma, C. C.; Wei, K. C. Magnetic Gold-Nanorod/ Pnipaamma Nanoparticles for Dual Magnetic Resonance and Photoacoustic Imaging and Targeted Photothermal Therapy. *Biomaterials* **2013**, *34* (22), 5651−5660.
(28) Xia, Y.; Li, W.; Cobley, C. M.; Chen, J.; Xia, X.; Zhang, Q.; Yang, M.; Cho, E. C.; Brown, P. K. Gold Nanocages: From Synthesis to Theranostic Applications. *Acc. Chem. Res.* **2011**, *44* (10), 914−924.
(29) Luo, H.; Xu, M.; Zhu, X.; Zhao, J.; Man, S.; Zhang, H. Lung Cancer Cellular Apoptosis Induced by Recombinant Human Endostatin Gold Nanoshell-Mediated near-Infrared Thermal Therapy. *FASEB J.* **2015**, *29* (1 Supplement), LB28.
(30) Yang, H.-J.; He, S.-Y.; Tuan, H.-Y. Self-Seeded Growth of Five-Fold Twinned Copper Nanowires: Mechanistic Study, Characterization, and Sers Applications. *Langmuir* **2014**, *30* (2), 602−610.
(31) Ye, E.; Zhang, S.-Y.; Liu, S.; Han, M.-Y. Disproportionation for Growing Copper Nanowires and Their Controlled Self-Assembly Facilitated by Ligand Exchange. *Chem. - Eur. J.* **2011**, *17* (11), 3074−3077.
(32) Veronese, F. M.; Mero, A. The Impact of Pegylation on Biological Therapies. *BioDrugs* **2008**, *22* (5), 315−329.
(33) Tian, Q.; Jiang, F.; Zou, R.; Liu, Q.; Chen, Z.; Zhu, M.; Yang, S.; Wang, J.; Wang, J.; Hu, J. Hydrophilic Cu9s5 Nanocrystals: A Photothermal Agent with a 25.7% Heat Conversion Efficiency for Photothermal Ablation of Cancer Cells in Vivo. *ACS Nano* **2011**, *5* (12), 9761−9771.
(34) Xu, Y.; Chen, D.; Jiao, X.; Xue, K. Nanosized Cu_2o/Peg400 Composite Hollow Spheres with Mesoporous Shells. *J. Phys. Chem. C* **2007**, *111* (44), 16284−16289.
(35) Roper, D. K.; Ahn, W.; Hoepfner, M. Microscale Heat Transfer Transduced by Surface Plasmon Resonant Gold Nanoparticles. *J. Phys. Chem. C* **2007**, *111* (9), 3636−3641.
(36) Habash, R. W.; Bansal, R.; Krewski, D.; Alhafid, H. T. Thermal Therapy, Part 1: An Introduction to Thermal Therapy. *Crit. Rev. Bioeng.* **2006**, *34* (6), 459−489.
(37) Kuo, C. W.; Lai, A. J.; Wei, K. H.; Chen, P. Studies of Surface-Modified Gold Nanowires inside Living Cells. *Adv. Funct. Mater.* **2007**, *17* (18), 3707−3714.
(38) Goode, A. E.; Gonzalez Carter, D. A.; Motskin, M.; Pienaar, I. S.; Chen, S.; Hu, S.; Ruenraroengsak, P.; Ryan, M. P.; Shaffer, M. S.; Dexter, D. T.; Porter, A. E. High Resolution and Dynamic Imaging of Biopersistence and Bioreactivity of Extra and Intracellular Mwnts Exposed to Microglial Cells. *Biomaterials* **2015**, *70*, 57−70.
(39) Chu, K. F.; Dupuy, D. E. Thermal Ablation of Tumours: Biological Mechanisms and Advances in Therapy. *Nat. Rev. Cancer* **2014**, *14* (3), 199−208.
(40) Bezu, L.; Gomes-de-Silva, L. C.; Dewitte, H.; Breckpot, K.; Fucikova, J.; Spisek, R.; Galluzzi, L.; Kepp, O.; Kroemer, G. Combinatorial Strategies for the Induction of Immunogenic Cell Death. *Front. Immunol.* **2015**, *6*, 187.
(41) Nogueira-Machado, J. A.; Volpe, C. M.; Veloso, C. A.; Chaves, M. M. Hmgb1, Tlr and Rage: A Functional Tripod That Leads to Diabetic Inflammation. *Expert Opin. Ther. Targets* **2011**, *15* (8), 1023−1035.
(42) Pittet, J. F.; Koh, H.; Fang, X.; Iles, K.; Christiaans, S.; Anjun, N.; Wagener, B. M.; Park, D. W.; Zmijewski, J. W.; Matthay, M. A.; Roux, J. Hmgb1 Accelerates Alveolar Epithelial Repair Via an Il-1β- and Avβ6 Integrin-Dependent Activation of Tgf-B1. *PLoS One* **2013**, *8* (5), e63907.
(43) Zhu, H.; Li, J.; Wang, S.; Liu, K.; Wang, L.; Huang, L. Hmgb1-Tlr4-Il-23-Il-17a Axis Promote Ischemia-Reperfusion Injury in a Cardiac Transplantation Model. *Transplantation* **2013**, *95* (12), 1448−1454.
(44) Gougeon, M. L.; Melki, M. T.; Saidi, H. Hmgb1, an Alarmin Promoting Hiv Dissemination and Latency in Dendritic Cells. *Cell Death Differ.* **2012**, *19* (1), 96−106.

DOI: 10.1021/acsami.6b04579
ACS Appl. Mater. Interfaces 2016, 8, 12082−12090